DOI 10.1007/s11182-017-1110-y

Russian Physics Journal, Vol. 60, No. 4, August, 2017 (Russian Original No. 4, April, 2017)

DISLOCATION SUBSTRUCTURES FORMED AFTER FRACTURE OF DEFORMED POLYCRYSTALLINE Cu–Al ALLOYS

N. A. Koneva, L. I. Trishkina, T. V. Cherkasova UDC 539.375.5

The paper deals with the dislocation substructure of polycrystalline FCC alloys modified by plastic deformation at a distance from the area of the specimen fracture. Observations are performed using the transmission electron microscopy. Cu–Al alloys with grain size ranging from 10 to 240 μm are studied in this paper. The parameters of the dislocation substructure are measured and their variation is determined by the increasing distance from the fracture area. It is shown how the grain size influences these processes. The different dislocation substructures which determine the specimen fracture at a mesocscale level are found herein.

Keywords: Cu–Al alloys, polycrystal, dislocation, substructure, deformation, fracture.

INTRODUCTION

As is known [1–5], the dynamic plastic deformation ε_{true} higher than 0.20–0.25, enables the creation of misoriented dislocation and dislocation-disclination substructures. These substructures include the formation of the interface with non-uniform misorientation, breaking sub-boundaries, bending-torsion amplitude of the crystal lattice, and internal stress fields. Dislocation-disclination substructures include microbands, one- and two-dimensional formations, fragments, subgrains, and also multivariable continuous and discrete misorientations. Previous studies focus on these types of substructures [6].

The fracture of metallic materials is a complicated process which is determined by the development of deformation at different scale levels [1]. During the investigation of the evolution of the dislocation substructure (DSS) with deformation, it is interesting to study the interaction between the fracture of materials having the dislocation-disclination substructures.

The aim of this paper is to explore the changes in the dislocation structure and its parameters at a distance from the specimen fracture and the identification of the its types which define the specimen fracture at a mesoscale level.

MATERIALS AND METHODS

FCC solid solutions of Cu-Al polycrystalline alloys were used in this experiment. Aluminum content was 0.5, 5, 10 and 14 at.%, the grain size varied between 10–240 μm. The alloy specimens were deformed at a room temperature and $2\cdot10^{-2}$ s^{-1} strain rate. Observations of the structure were made on a transmission electron microscope (TEM) goniometer at 125 kV accelerating voltage and ×30000 magnification. The dislocation structure and its parameters were investigated in the specimen at $2\cdot10^{-3}$ m distance from its fracture area. The degree of the local deformation ε^{l}_{true} was detected for each local area of the specimen. TEM images were used to measure the DSS parameters using the secant method [7], namely: the size of the dislocation cells, the width of the dislocation cell walls, the sub-boundary density,

Tomsk State University of Architecture and Building, Tomsk, Russia, e-mail: koneva@tsuab.ru; trishkina.53@mail.ru; cherkasova_tv@mail.ru. Translated from Izvestiya Vysshikh Uchebnykh Zavedenii, Fizika, No. 4, pp. 14–19, April, 2017. Original article submitted January 19, 2017.

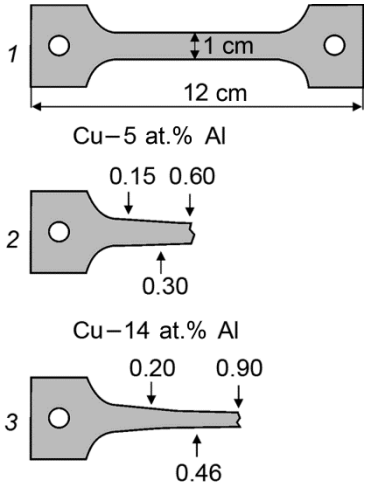

Fig. 1

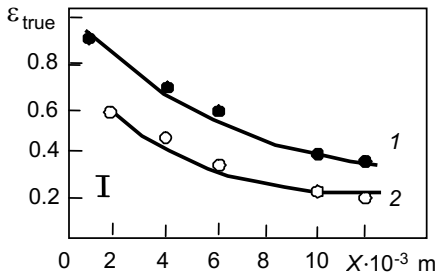

Fig. 2

Fig. 1. Schematic view of specimens: *1* – original state, *2*, *3* – after fracture. Fractional numbers indicate local deformation degrees.

Fig. 2. Deformation degree in Cu alloys at *X* distance form the fracture area: *1* – 10–14 at.% Al; *2* – 0.5– 5 at.% Al.

the microband density, the density of microkracks. The bending-torsion amplitude was determined in these local areas using the bend extinction contours [8, 9] which indicate the formation of internal stress fields. The bending-torsion amplitude can be obtained from the gradient of continuous misorientation [8, 9]:

$$\chi = \frac{\partial \varphi}{\partial \ell},$$

where φ is the angle of inclination of the crystallographic plane relative to the electron beam; ℓ is the distance on the plane. The detail measurements of $\Delta\varphi / \Delta\ell$ ratio are given in [8, 10].

RESULTS AND DISCUSSION

Two types of specimens shown in Fig. 1 are investigated before and after their fracture. Thus, the alloy specimens with Al content below 5 at.% fractured at $\varepsilon_{true} = 0.60$, whereas alloys with higher Al concentration (8–14 at.%) fractured at $\varepsilon_{true} = 0.90$. In Fig. 2, one can see the degree of local deformation in different specimen areas at *X* distance from their fracture area.

Let us consider the dislocation structures observed with increasing distance from the fracture area in Cu alloys having 0.5 and 5 at.% Al and 100 μm grain size. In Cu–0.5 at.% Al alloys ($\varepsilon^{l}_{true} = 0.60$), the dislocation substructure is observed to be misoriented and fragmented. TEM images shown in Fig. 3, present the DSS observed in this alloy. With increasing distance from the fracture area, the DSS formation has the following sequence: fragmented → misoriented → non-misoriented cellular. The similar DSS are also observed in this alloy having other grain size.

Starting from the fracture area, the average scalar dislocation density, dislocation densities of non-misoriented and misoriented cellular substructures, in cell walls and inside cells, the bending-torsion amplitude, the density of breaking sub-boundaries and microcracks are measured in different parts of the specimen. The analysis of the obtained data allows us to describe the dislocation structure depending on the increasing distance from the fracture area.

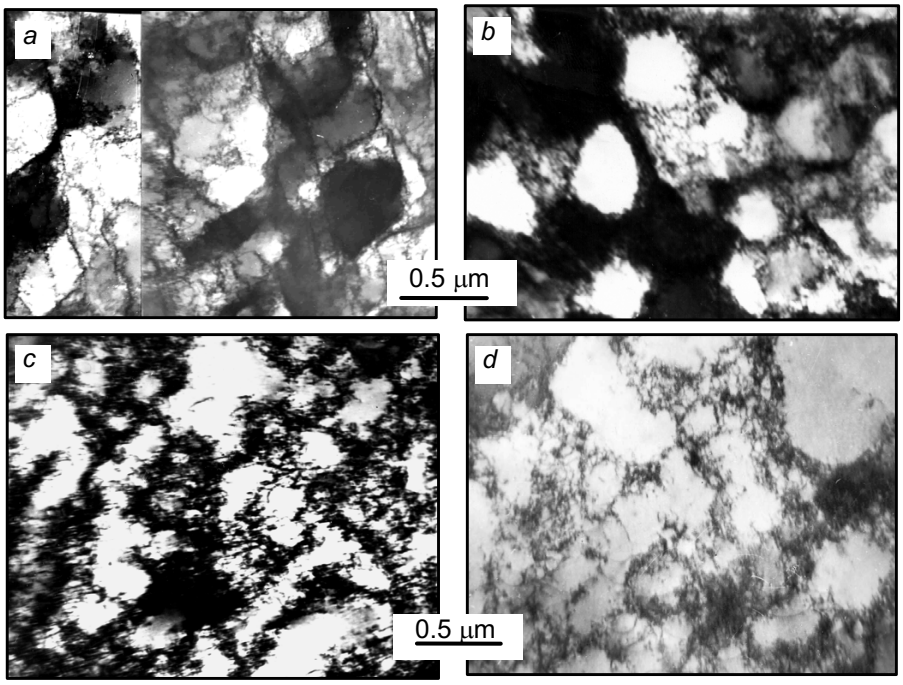

Fig. 3. TEM images of Cu alloy substructures at different distances from fracture area relevant to ε^{l}_{true} values at 0.5 at.% Al: *a*, *b* – $\varepsilon^{l}_{true} = 0.60$ ($X = 2 \cdot 10^{-3}$ m); *c*, *d* – $\varepsilon^{l}_{true} = 0.40$ ($X = 6 \cdot 10^{-3}$ m); *a* – fragmented, *b*, *c* – misoriented cellular; *d* – non-misoriented cellular.

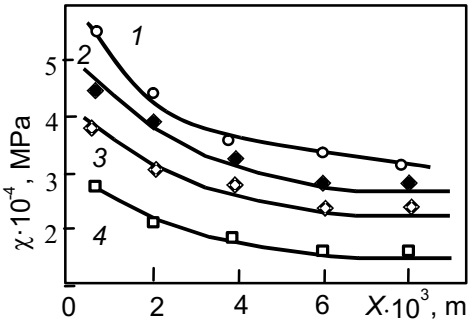

Fig. 4. Variation in bending-torsion amplitude as a function of the distance from the fracture area at different degrees of deformation in Cu–0.5 at.% Al alloy in different locations: *1* – nearby grain boundaries; *2* – nearby breaking sub-boundaries; *3* – in fragmented DSS; *4* – in misoriented cellular DSS. (100 μm grain size).

Figure 4 presents the diagram for the bending-torsion amplitude χ with increasing distance from the fracture area in the specimen with 0.5 at.% Al content. As can be seen from Fig. 4, χ value decreases with the increase in the distance *X*. Thus, it becomes higher nearby the fracture area, and in the vicinity of grain boundaries the bending-torsion amplitude χ achieves its maximum. Breaking sub-boundaries and fragmented DSS are also characterized by a higher bending-torsion amplitude. It is worth noting that to a distance of $4 \cdot 10^{-3}$ m from the fracture area, the χ value reduces more intensively than with further increase in the distance from it. As can be seen, when the distance *X* continues to

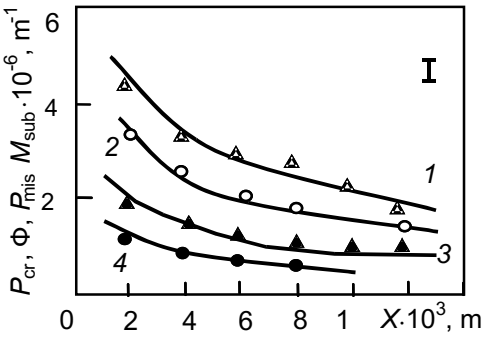

Fig. 5. Variation in misoriented DSS parameters as a function of the distance from the fracture area in Cu–0.5 at.% Al alloy: *1* – density P_{mis} of misoriented cell boundaries; *2* – density F of fragments; *3* – density M_{sub} of breaking sub-boundaries; *4* – density P_{cr} of microcracks. (100 μm grain size).

grow, $\chi = f(X)$ dependence becomes practically constant. With increasing distance from the fracture area, the cell size and the width of their cells increase, while the dislocation density decreases.

The variation in misoriented DSS parameters and the distance from the fracture area in Cu–0.5 at.% Al alloy is shown in Fig. 5. Nearby the fracture area, the density of breaking sub-boundaries, misoriented cell boundaries, fragments and microcracks is the highest, and with increasing distance from the fracture area, it decreases and becomes practically constant.

In [11] it was shown that the increase in Al content in Cu–Al alloys reduces the stacking fault energy, thereby leading to the formation of other DSS due to plastic deformation [12]. The formation of misoriented cellular network, microband and microtwin substructures occurs in Cu alloys with 10 at.% Al and 14 at.% Al during the developed plastic deformation. Fine-scale twinning is observed in three crystallographic directions resulting in the formation of microtwin bundles. In these microtwin bundles, bend extinction contours positioned between lamellas, are mostly perpendicular to the microtwins.

Microtwins are often bended. The different types of DSS are shown in Fig. 6 for Cu–14 at.% Al alloy sequenced depending on the distance from the fracture area, *i.e.* microtwins (*a*) → microbands (*b*) → misoriented cellular network in one microtwin direction (*c*, *d*), microband and misoriented cellular and network (*e*), non-misoriented cellular (*f*). Microcracks nucleate in the material along the microtwin boundaries (*c*). At the deformation degree of $\varepsilon^{l}_{true} > 0.20$, the extinction contours are observed in each DSS type that indicates to the bending and torsion of the crystal lattice.

The variation in bending-torsion amplitude with the increasing distance from the fracture area is plotted in Fig. 7 for Cu–14 at.% Al alloy nearby the microcracks, grain boundaries, misoriented cellular and microband DSS. As can be seen, with increasing distance from the fracture area, the bending-torsion amplitude χ uniformly decreases. The higher χ values are observed nearby microcracks, grain boundaries and microtwins.

The grain size has a significant effect on the DSS parameters and the specimen fracture. Microcracks locate along the grain boundaries. According to Fig. 8, the bending-torsion amplitude reduces in the fracture area with the increase in the grain size from 10 to 100 μm. A further increase in the grain size has no a notable effect on χ value. It is worth mentioning here that the larger grain size the higher plasticity of the alloy. In alloys high in Al, the bending-torsion amplitude χ is larger than in alloys with low Al concentration. The causes of this phenomenon are not discussed in this work.

It is reasonable to conclude from this analysis that at the moment of the specimen fracture, the plastic deformation becomes rather inhomogeneous (see Fig. 2). Inhomogeneous deformation correlates with the observed DSS parameter gradient depending on the distance from the fracture area. In alloys low in Al, the density of misoriented boundaries (cells and fragments) turns to be the highest within the fracture area. Microcracks develop along these boundaries and their density is also the highest near the fracture area. The boundaries of misoriented cells and fragments

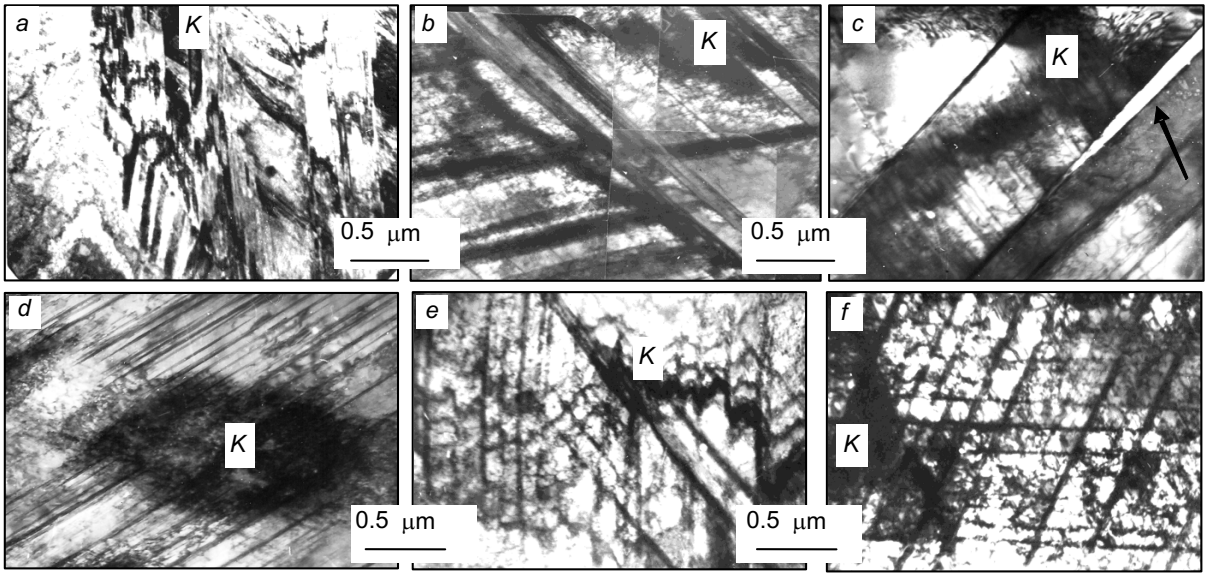

Fig. 6. TEM images of Cu–14 at.% Al alloy defect structure at different distances from fracture area: *a–c* – $2 \cdot 10^{-3}$ m; *d–e* – $6 \cdot 10^{-3}$ m; *a* – three microtwin directions; *b* – microband DSS; *c* – microcrack (emphasized by black arrow) along microtwin boundary; *d* – one microtwin direction; *e* – microband and misoriented cellular and network; *e* – misoriented cellular DSS; *K* – extinction contours. (100 μm grain size).

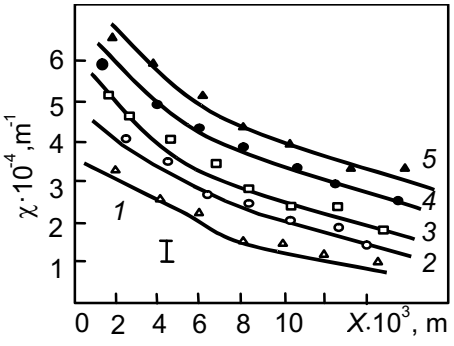

Fig. 7

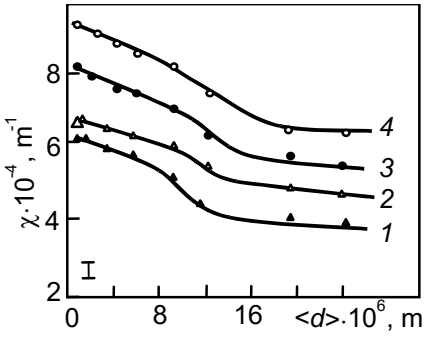

Fig. 8

Fig. 7. Variation in bending-torsion amplitude as a function of the distance from fracture area in Cu–14 at.% Al alloy: misoriented cellular network DSS (curve *1*); microband DSS (curve *2*); nearby microtwins (curve *3*); along grain boundaries (curve *4*); along microcrack boundaries (curve *5*).

Fig. 8. Relationship between the bending-torsion amplitude and the grain size for Cu alloys with different Al content: *1* – 0.5 at.%; *2* –5 at.%; *3* –10 at.%; *4* – 14 at.%.

induce the bending-torsion amplitude of the crystal lattice and, as consequence, internal stress fields which achieve their maximum in the vicinity of the fracture area. All these factors facilitate the fracture of the specimen at a mesoscale level. Panin *et al.* [13, 14] studied the crystalline structure and showed that the crack propagation during the material fracture is determined by the local bending of the crystal lattice appeared at different scale levels.

In alloys with high Al content, the formation of the two DSS types is observed, namely microtwins and microbands. The highest density of misoriented boundaries (microbands) is detected within the fracture area. The formation of microcracks is detected along the microbands. The density of microtwins is also significant within the fracture area where microcracks originate from. The crack formation along the grain boundaries is common to each of the investigated alloys.

CONCLUSIONS

In conclusion, it is evident that this study has shown the formation of the dislocation substructure in the local areas of polycrystalline Cu–Al alloys at the moment of the specimen fracture. The types of the dislocation subtructure were determined at different distances from the fracture area. The DSS parameters and their gradient variations were obtained depending on the distance from the fracture area.

The results suggest that in all the investigated alloys, nearby the fracture area, the observed deformation-misoriented boundaries have the maximum bending-torsion amplitude of the crystal lattice. In alloys with a low Al content misoriented boundaries represented fragments and cells, whereas in alloys high in Al, microtwins and microbands were found.

It should be also concluded that the misoriented boundaries in each of the investigated alloys with a large bending-torsion amplitude of the crystal lattice determined the fracture of material at a mesoscale level. Another source of the crack formation at this level is the grain boundary. So, the decrease in plasticity of Cu-Al alloys depends on the decrease in their grain size.

This work was carried out within the government contract N 3.8320.2017/BCh of the Ministry of Education and Science of the Russian Federation.

REFERENCES

1. V. V. Rybin, Large-Scale plastic Deformations and Fracture of Metals [in Russian]. Metallurgiya, Moscow (1986).
2. V. I. Trefilov, V. F. Moiseev, E. P. Pechkovskii, *et al*. Deformation Hardening and Fracture of Polycrystalline Materials [in Russian]. Naukova dumka, Kiev (1989).
3. N. A. Koneva, D. V. Lychagin, L. A. Teplyakova, and É. V. Kozlov, Theoretical and Experimental Research of Disclinations [in Russian]. Ioffe Physical-Technical Institute of the Russian Academy of Sciences, Leningrad (1986), pp. 116–126.
4. N. A. Koneva and É. V. Kozlov, Structural Levels of Plastic Deformation and Fracture [in Russian]. Nauka, Novosibirsk (1990), pp. 123–186.
5. É. V. Kozlov, N. A. Koneva, and L. I. Trishkina, Dislocation and Rotational Deformation of Solids [in Russian]. Ioffe Physical-Technical Institute of the Russian Academy of Sciences, Leningrad (1990), pp. 89–125.
6. N. A. Koneva, É. V. Kozlov, and L. I. Trishkina, Metallofizika, **13**, No. 10, 49– 58 (1991).
7. S. A. Saltykov, Stereometric Metallography [in Russian]. Metallurgiya, Moscow (1970).
8. N. A. Koneva, L. I. Trishkina, D. V. Lychagin, and É. V. Kozlov, New Methods in Physics and Mechanics of Deformable Solids [in Russian]. Pt. 1, E. Panin, ed., TSU, Tomsk (1990), pp. 83–93.
9. N. A. Koneva, L. I. Trishkina, T. V. Cherkasova, and É. V. Kozlov, Vestnik Tambovskogo universiteta. Ser. Estestvennye i Tekhnicheskie Nauki, **21**, No. 3, 726–729 (2016).

10. É. V. Kozlov, D. V. Lychagin N. A. Koneva, and L. I. Trishkina, Strength Physics of Heterogeneous Materials [in Russian]. A. Romanov, ed., Ioffe Physical-Technical Institute of the Russian Academy of Sciences, Leningrad (1988), pp. 3–13.
11. A. Howie and P. R. Swaon, Phil. Mag., No. 6, 1215–1226 (1961).
12. N. A. Koneva, É. V. Kozlov, L. I. Trishkina, and T. V. Cherkasova, FPSM, **13**, No. 2, 162–167 (2016).
13. V. E. Panin, A. V. Panin, T. F. Elsukova, and Yu. F. Popkova, Phys. Mesomech., **17**, No. 6, 7–18 (2014).
14. V. E. Panin, V. E. Egorushkin, A. V. Panin, and A. G. Chernyavskii, Phys. Mesomech., **19**, No. 1, 31–46 (2016).